Recent Developments in the Flux Reconstruction Method

Joshua Romero, PhD candidate
Kartikey Asthana, PhD candidate
Jonathan Bull, Postdoctoral Scholar
Antony Jameson, Professor
Aerospace Computing Laboratory, Stanford University

AFOSR Computational Math Meeting
Arlington, VA July 28-30 2014

Acknowledgements

The research presented has been made possible by the support of the following organizations:

- Airforce Office of Scientific Research under grant FA9550-10-1-0418 by Dr. Fariba Fahroo
- National Science Foundation under grant 1114816 monitored by Dr. Leland Jameson
- Thomas V Jones Stanford Graduate Fellowship
- National Science Foundation Graduate Fellowship

Outline

Outline

Flux Reconstruction (FR) Method

- Unifying framework that recovers several popular Discontinuous Finite Element methods:
  - Nodal Discontinuous Galerkin (nodal DG)
  - Spectral Difference (SD)
- Energy Stable Flux Reconstruction (ESFR) formulation proven to be linearly stable for advection-diffusion problems

Review of Existing Methodology

Consider a 1D scalar conservation law:

$$\frac{\partial u}{\partial t} + \frac{\partial f(u)}{\partial x} = 0$$

Represent solution and flux within each element using Lagrange interpolating polynomials through $P+1$ interior solution points. Resulting polynomials are of order P.

$$u_j(r) = \sum_{n=1}^{P+1} u_n l_n$$

$$f_j(r) = \sum_{n=1}^{P+1} f_n l_n$$

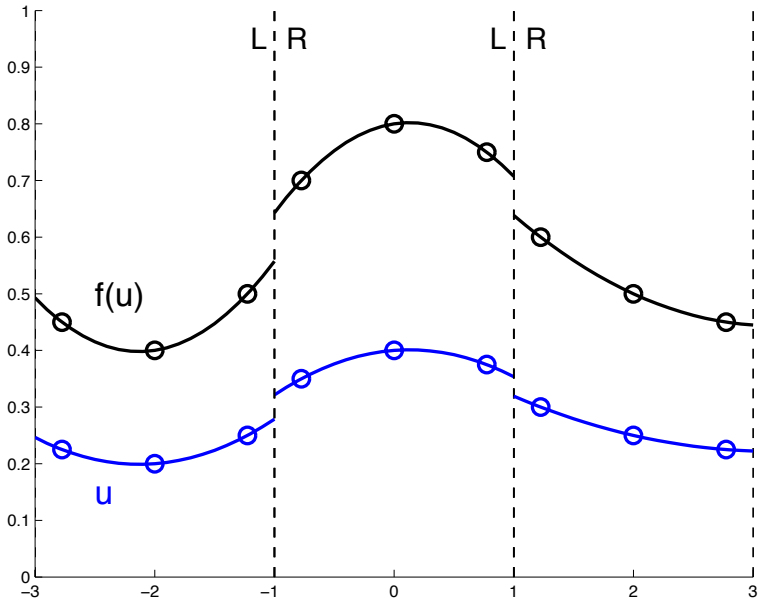

Review of Existing Methodology

From left and right solution values at each interface, compute a common interface flux using an appropriate flux formulation.

$$f_L^I = \text{fcn}(u_{j-1,R}, u_{j,L})$$
$$f_R^I = \text{fcn}(u_{j,R}, u_{j+1,L})$$

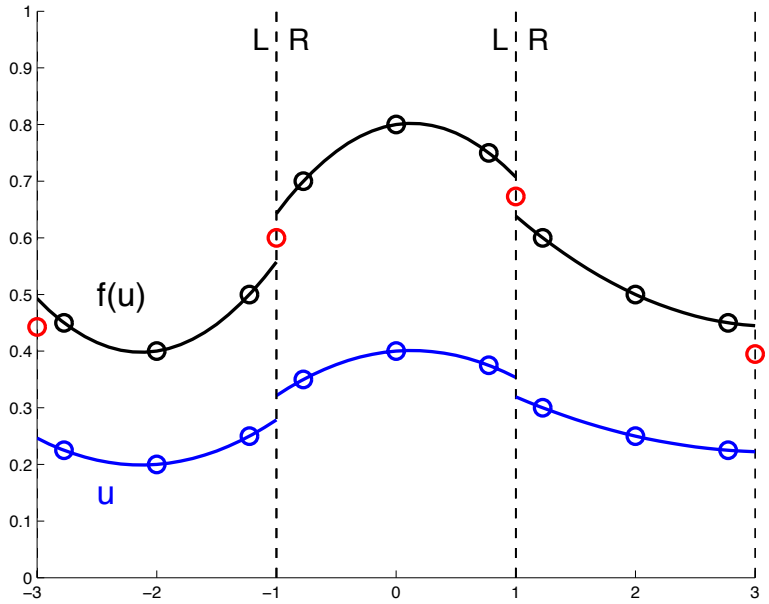

Review of Existing Methodology

Acquire values of the discontinuous flux at interfaces using existing Lagrange representation.

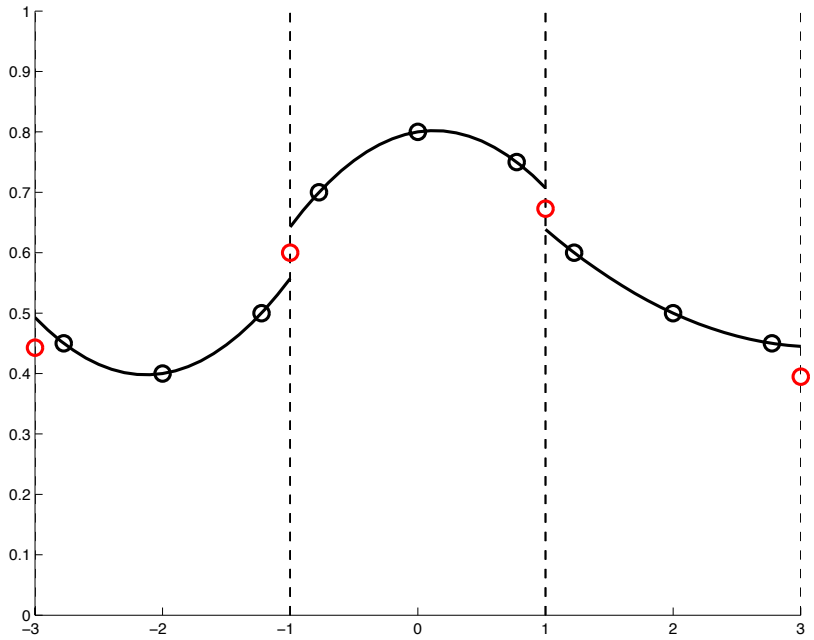

Degree P

Review of Existing Methodology

Acquire values of the discontinuous flux at interfaces using existing Lagrange representation.

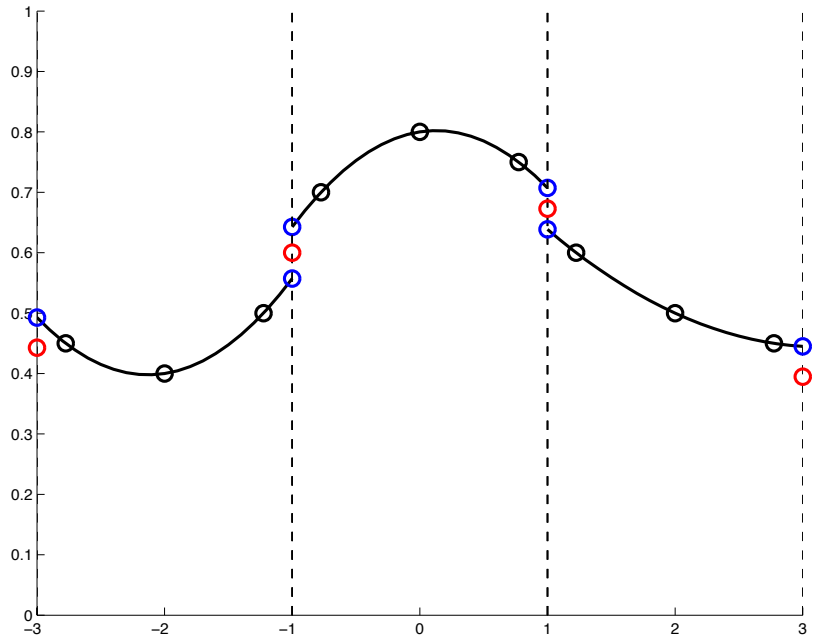

Degree P

Review of Existing Methodology

Introduce left and right correction polynomials of degree $P + 1$.

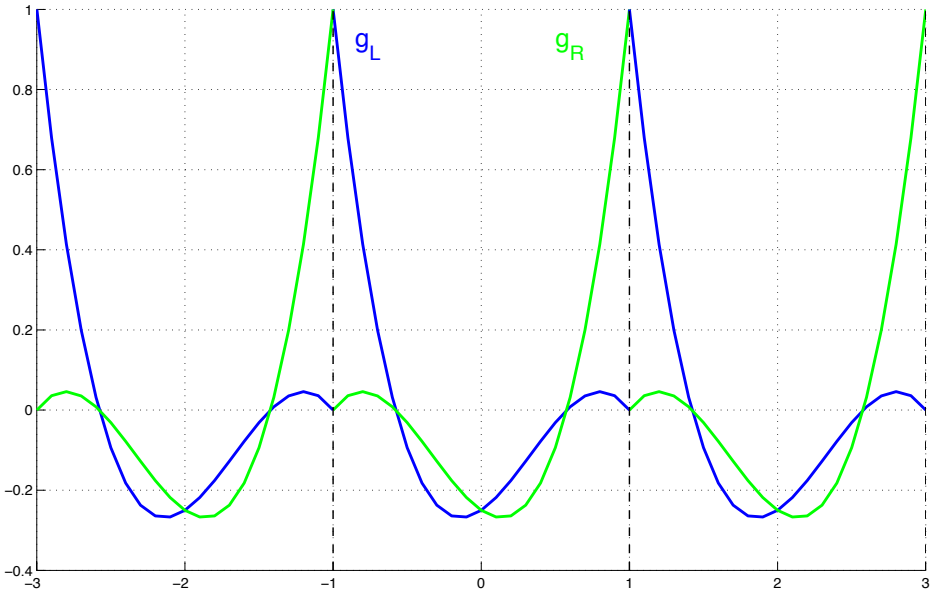

Review of Existing Methodology

Scale polynomials using computed difference between desired common interface flux value and existing discontinuous flux value.

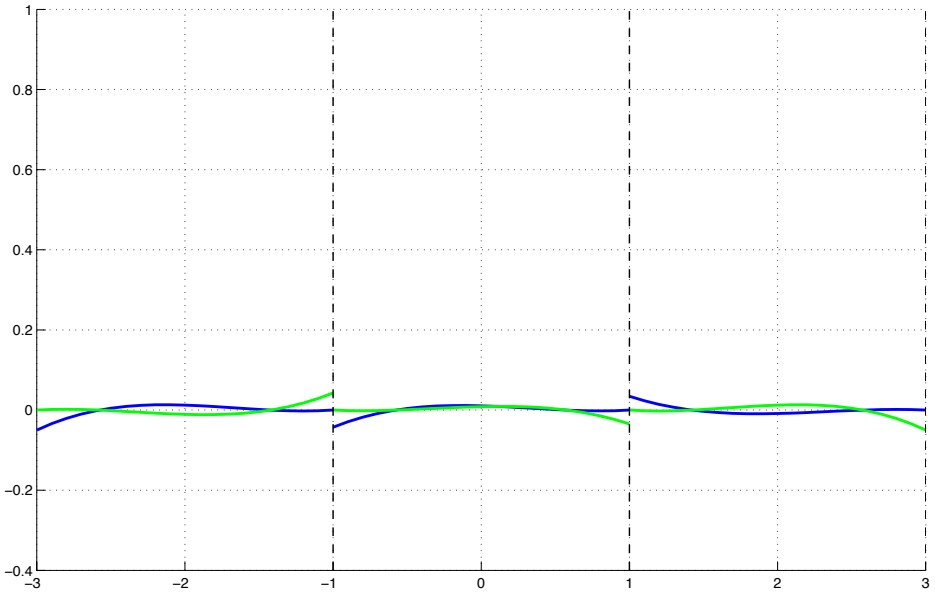

Review of Existing Methodology

Add the scaled correction polynomials to the discontinuous flux to obtain a C-0 continuous flux of order $P+1$.

$$f_j^c(r) = f_j(r) + (f_L^I - f_j(-1))g_L(r) + (f_R^I - f_j(+1))g_R(r)$$

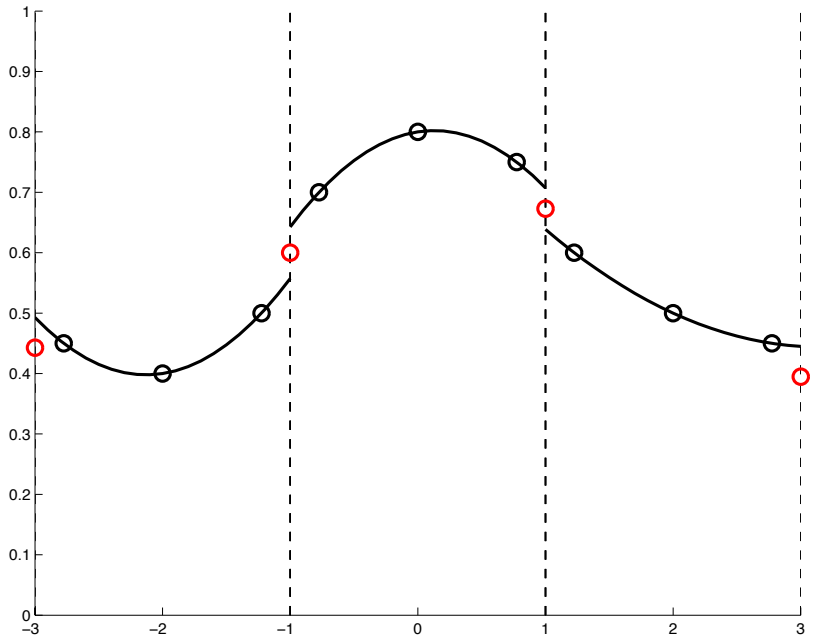

Degree P

Review of Existing Methodology

Add the scaled correction polynomials to the discontinuous flux to obtain a C-0 continuous flux of order $P+1$.

$$f_j^c(r) = f_j(r) + (f_L^I - f_j(-1))g_L(r) + (f_R^I - f_j(+1))g_R(r)$$

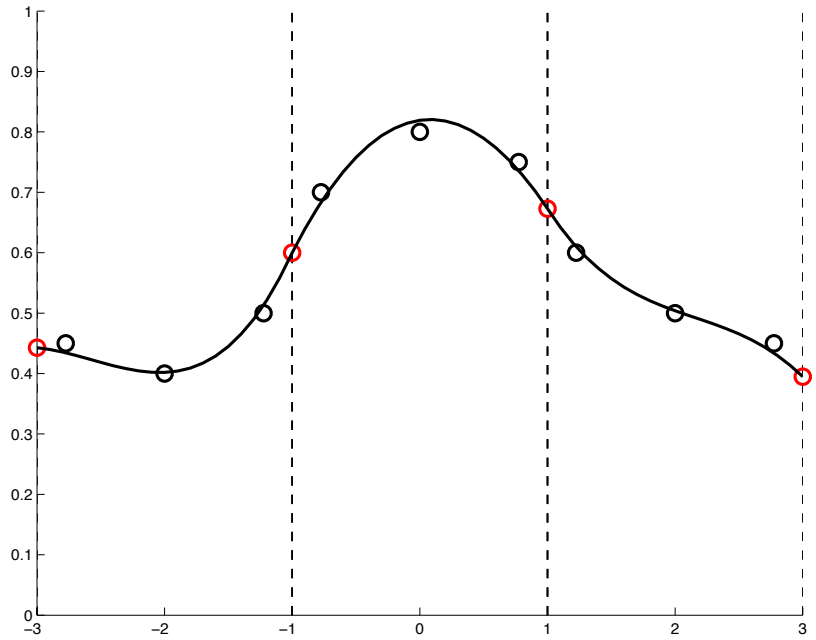

Degree $P+1$

Review of Existing Methodology

Advance solution using derivative of the continuous flux.

$$\frac{d}{dt}\mathbf{u_j} = -[\mathbf{D}\mathbf{f}_j + l_L\mathbf{g_L}_{,\mathbf{x}} + l_R\mathbf{g_R}_{,\mathbf{x}}]$$

New Developments in Flux Reconstruction

- While existing FR methodology has shown much promise, active research is still being conducted to characterize and improve the method.
- From this research, several exciting new developments have emerged:
  - **Direct FR** - Simplified formulation of the FR method that recovers nodal discontinuous Galerkin (DG) method
  - **Spectrally Optimal FR Schemes** - New schemes that minimize wave propagation errors for the range of resolvable wavenumbers

Outline

Direct FR Method

- In existing FR method, reconstruction process involves several distinct computational steps, all aimed at applying correction polynomials to construct the continuous flux.
- Correction polynomials introduced by Huynh to generate continuous flux of order $P+1$ so that terms in conservation law are of consistent order P.

Direct FR Method

If this consistency constraint is abandoned, entire reconstruction process can be consolidated into a single Lagrange interpolation through the combined set of interior solution points and interface flux points.

$$f^C = f_L^I \tilde{l}_0 + \sum_{n=1}^{P+1} f_n \tilde{l}_n + f_R^I \tilde{l}_{P+2}$$

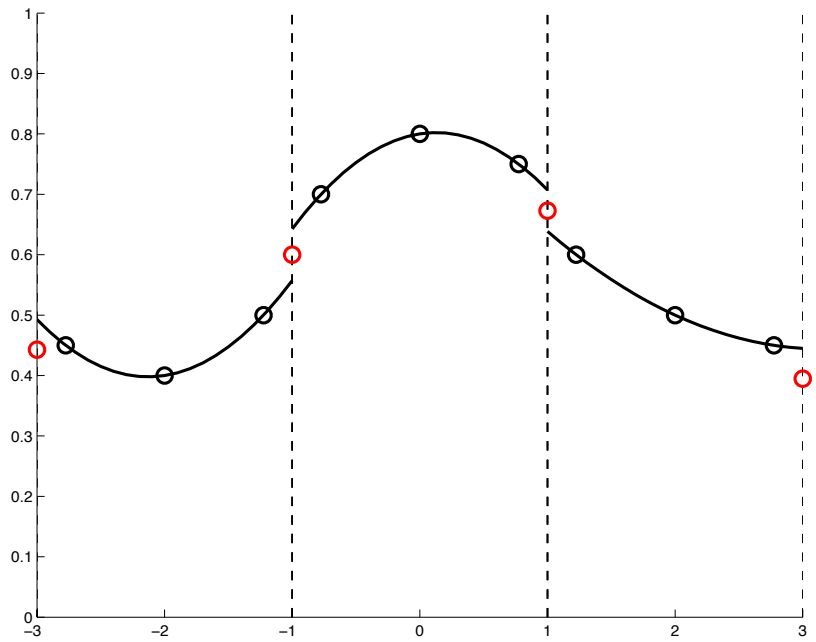

Degree P

Direct FR Method

If this consistency constraint is abandoned, entire reconstruction process can be consolidated into a single Lagrange interpolation through the combined set of interior solution points and interface flux points.

$$f^C = f_L^I \tilde{l}_0 + \sum_{n=1}^{P+1} f_n \tilde{l}_n + f_R^I \tilde{l}_{P+2}$$

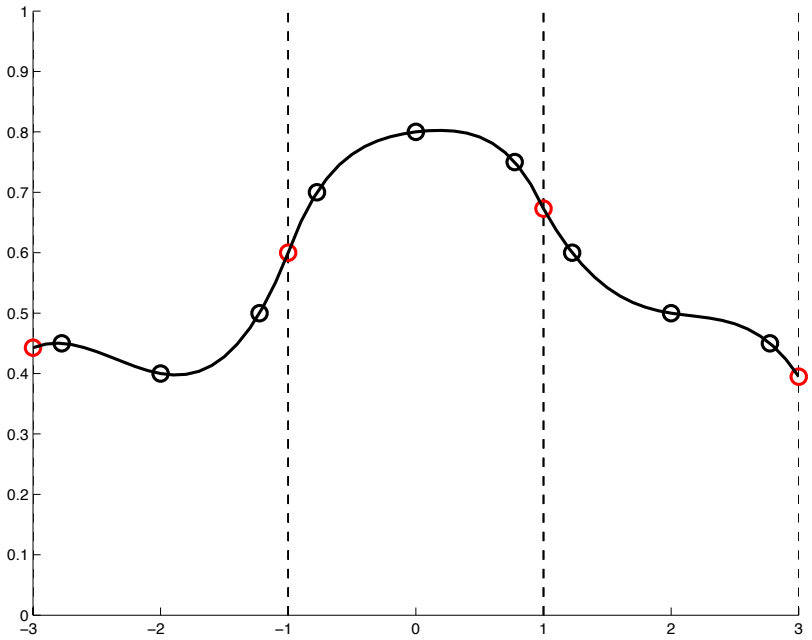

Degree $P + 2$

Advantages of the New Formulation

- **Simpler** - Does not require explicit definition of correction functions, implicit through selection of solution points
- **Cheaper** - Less operations than existing FR methodology
- **Equivalent** - Recovers nodal DG scheme if solution points are positioned at the zeros of the Legendre polynomial of corresponding order
  - Maintains linear stability properties of this scheme
- **Potential for new family of schemes** - Numerical results indicate that schemes derived through positioning the solution points at the zeros of Jacobi polynomials (with some constraints) are linearly stable.

Equivalency Requirements

- Solution update is only computed and applied discretely at interior solution points
- DFR can be made to recover the nodal DG scheme if the following condition is met on the total continuous flux:

$$\frac{\partial}{\partial r}(f(r) - f_{DFR}(r))\bigg|_{r=r_j} = 0$$

for $j = 1, ..., P+1$ which are the indices spanning only the interior solution points.

$$f(r) = f^D(r) + f^C(r)$$

Equivalency Requirements

It can be found that this equivalency requirement can be cast equivalently using only the correction fluxes:

$$\frac{\partial}{\partial r}(f^C(r) - f^C_{DFR}(r))\Big|_{r=r_j} = 0 \tag{1}$$

for $j = 1, ..., P+1$

Proof of Equivalency to Nodal DG

Consider splitting the DFR correction flux using effective left and right correction functions, $g_{L\,DFR}$ and $g_{R\,DFR}$

$$f^C_{DFR}(r) = \Delta f_L g_{L\,DFR}(r) + \Delta f_R g_{R\,DFR}(r) \tag{2}$$

and compare to the equivalent formula from the standard FR method

$$f^C(r) = \Delta f_L g_L(r) + \Delta f_R g_R(r) \tag{3}$$

Proof of Equivalency to Nodal DG

Subtracting Eq.(3) and Eq.(2), taking a derivative, and substituting results from Eq.(1) gives

$$\Delta f_L \frac{\partial}{\partial r}(g_L(r) - g_{L_{DFR}}(r))\Big|_{r=r_j} + \Delta f_R \frac{\partial}{\partial r}(g_R(r) - g_{R_{DFR}}(r))\Big|_{r=r_j} = 0$$

Since Δf_L and Δf_R are arbitrary, it suffices to prove

$$\frac{\partial}{\partial r}(g_L(r) - g_{L_{DFR}}(r))\Big|_{r=r_j} = 0 \tag{4}$$

$$\frac{\partial}{\partial r}(g_R(r) - g_{R_{DFR}}(r))\Big|_{r=r_j} = 0 \tag{5}$$

to prove scheme equivalency.

Proof of Equivalency to Nodal DG

It is known that to recover the nodal DG scheme using the standard FR methodology requires correction functions of the form

$$g_L = \frac{(-1)^P}{2}(L_P - L_{P+1}) \tag{6}$$

$$g_R = \frac{1}{2}(L_P + L_{P+1}) \tag{7}$$

which are the left and right Radau polynomials respectively.
If the interior solution points using the DFR scheme are located at the zeros of the Legendre polynomial, the effective DFR correction functions that results from the Lagrange interpolation can be expressed in terms of Legendre polynomials as

$$g_{L_{DFR}} = \frac{(-1)^P}{2}(r-1)L_{P+1} \tag{8}$$

$$g_{R_{DFR}} = \frac{1}{2}(1+r)L_{P+1} \tag{9}$$

Proof of Equivalency to Nodal DG

To satisfy Eq.(5), consider a residual defined as

$$D = \frac{\partial}{\partial r}(g_R - g_{R\,DFR}) = \frac{1}{2}(\frac{\partial}{\partial r}L_P - L_{P+1} - r\frac{\partial}{\partial r}L_{P+1}) \tag{10}$$

According to A.9 in Huynh (2007)

$$(1-r^2)\frac{\partial}{\partial r}L_{P+1} = (P+1)\left[L_p - rL_{P+1}\right] \tag{11}$$

Substitution into Eq.(10) yields

$$D = \frac{1}{2(1-r^2)}\left[(1-r^2)(\frac{\partial}{\partial r}L_P - L_{P+1}) - (P+1)(rL_P - r^2L_{P+1})\right] \tag{12}$$

Proof of Equivalency to Nodal DG

According to A.10 in Huynh (2007)

$$(1 - r^2)\frac{\partial}{\partial r} L_P = (P + 1)(rL_P - L_{P+1}) \tag{13}$$

Substitution into Eq.(12) yields

$$D = -\frac{1}{2}(P + 2)L_{P+1} \tag{14}$$

At the zeros of L_{P+1}, which correspond to the locations of the interior solution points, the residual is exactly equal to zero and Eq.(5) is satisfied.

Proof of Equivalency to Nodal DG

Eq.(4) can be satisfied in similar fashion. Consider a residual defined as

$$D = \frac{\partial}{\partial r}(g_L - g_{L_{DFR}}) = \frac{(-1)^P}{2}(\frac{\partial}{\partial r}L_P - L_{P+1} - r\frac{\partial}{\partial r}L_{P+1}) \tag{15}$$

Observing that the bracketed term in Eq.(15) is identical to the term in Eq.(10), it can be immediately said that

$$D = \frac{(-1)^{P+1}}{2}(P+2)L_{P+1} \tag{16}$$

At the zeros of L_{P+1}, which correspond to the locations of the interior solution points, the residual is exactly equal to zero and Eq.(4) is also satisfied. This proves the equivalence of the DFR scheme to the FR formulation of the nodal DG scheme provided the solution points are located at the zeros of the Legendre polynomial of order $P+1$.

Comparison of Correction Functions for $P = 2$

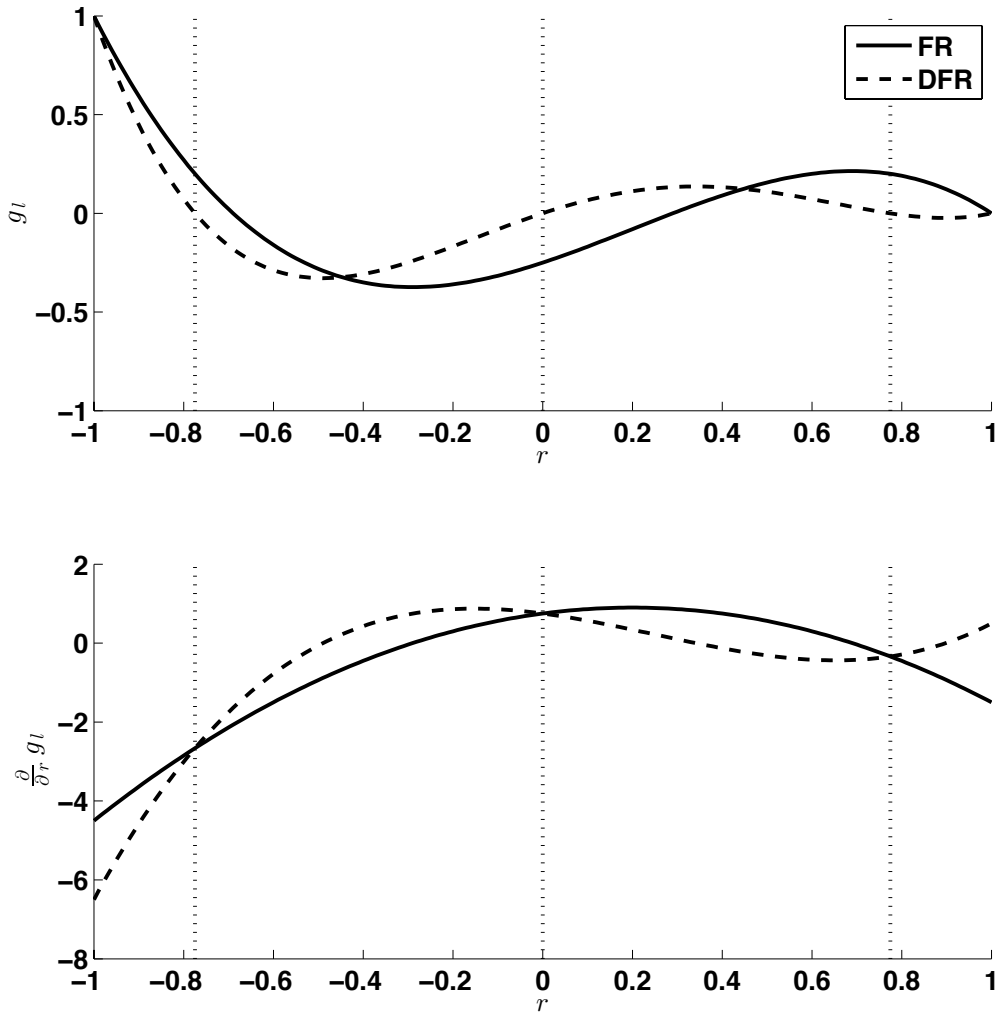

Comparison of Correction Functions for $P = 4$

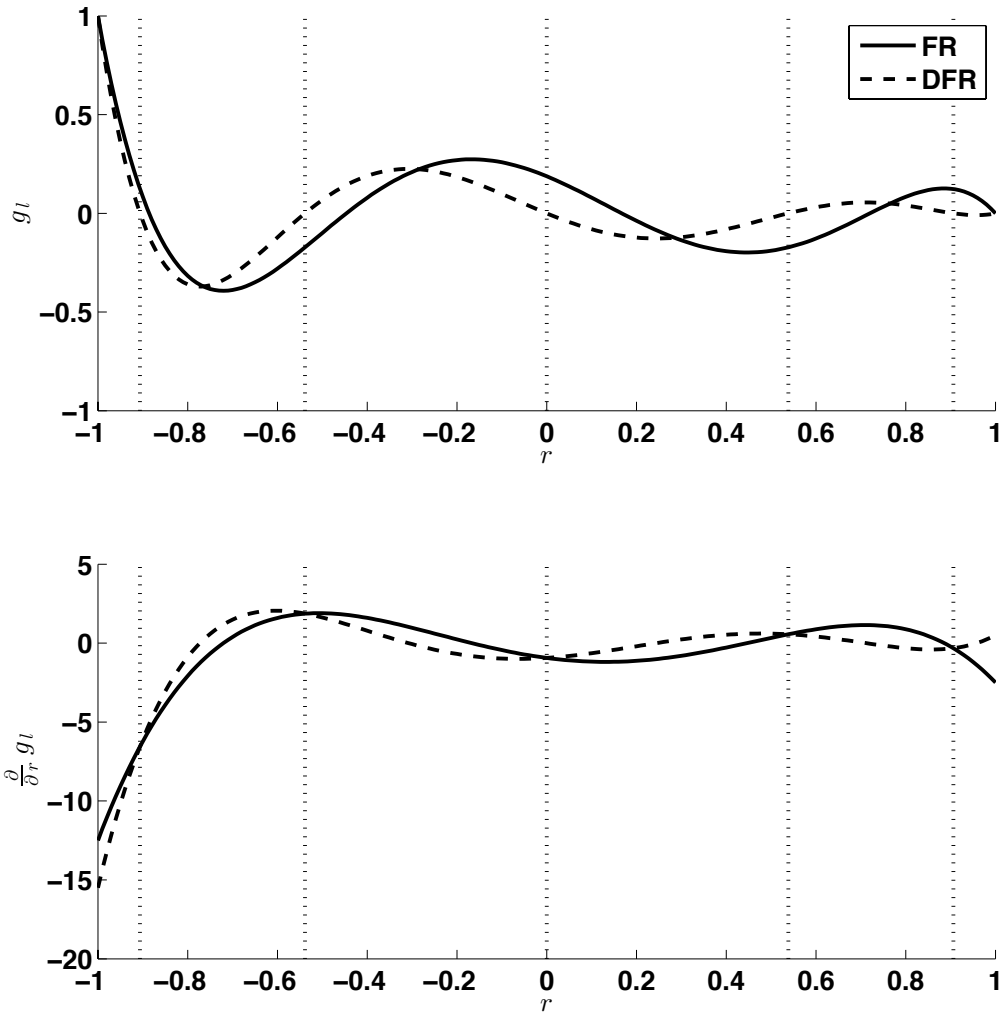

2D Euler: Isentropic Vortex

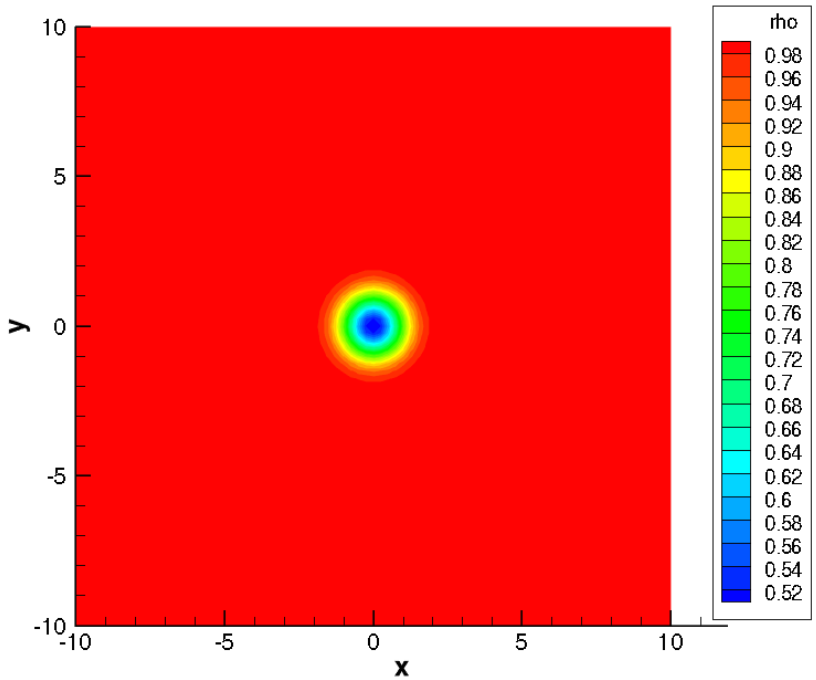

Test Case Parameters:

- $P = 4$
- 10K Degrees of Freedom
- $dt = 0.01$
- 6000 Iterations ($t = 60$)

2D Euler: Isentropic Vortex

FR (nodal DG):

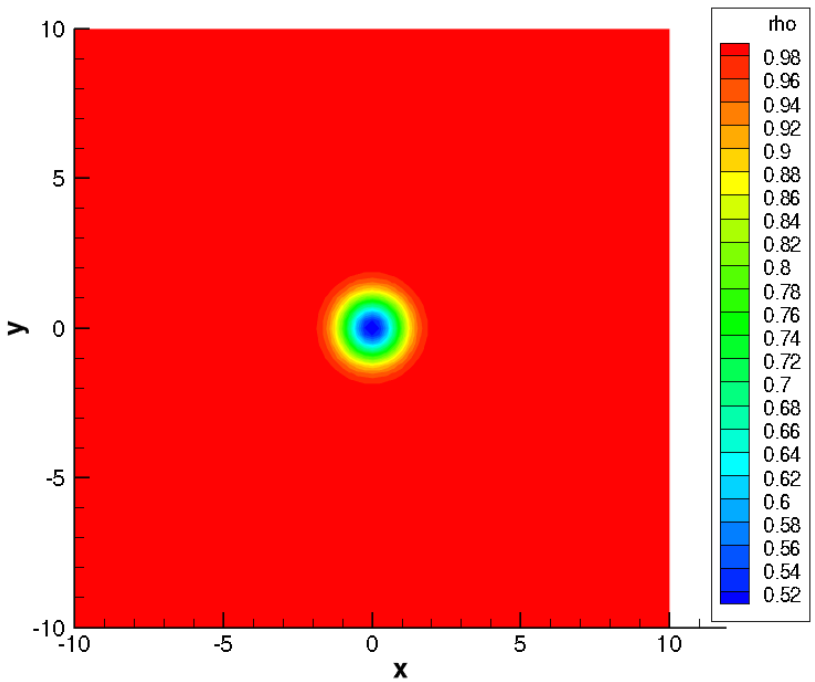

Direct FR:

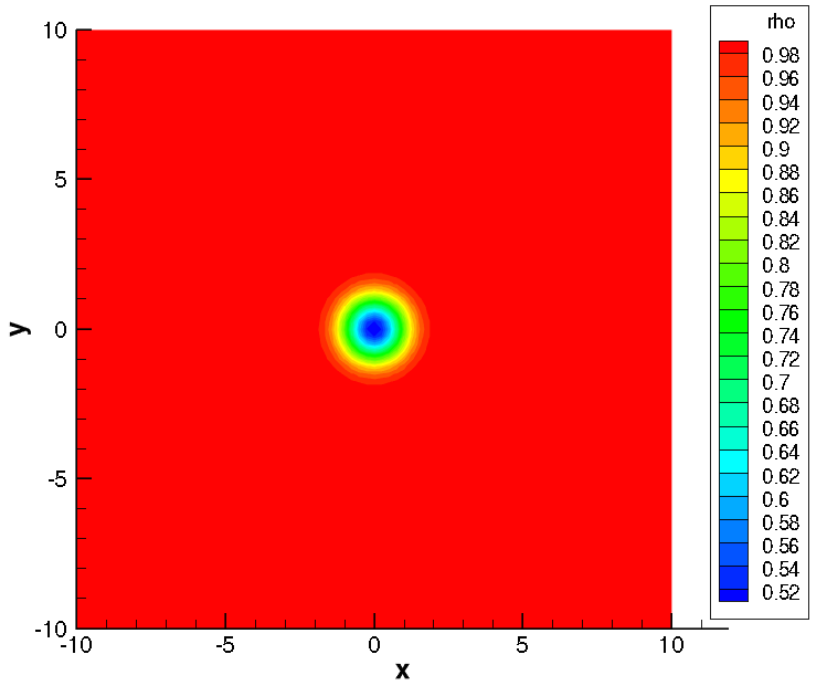

2D Euler: Isentropic Vortex

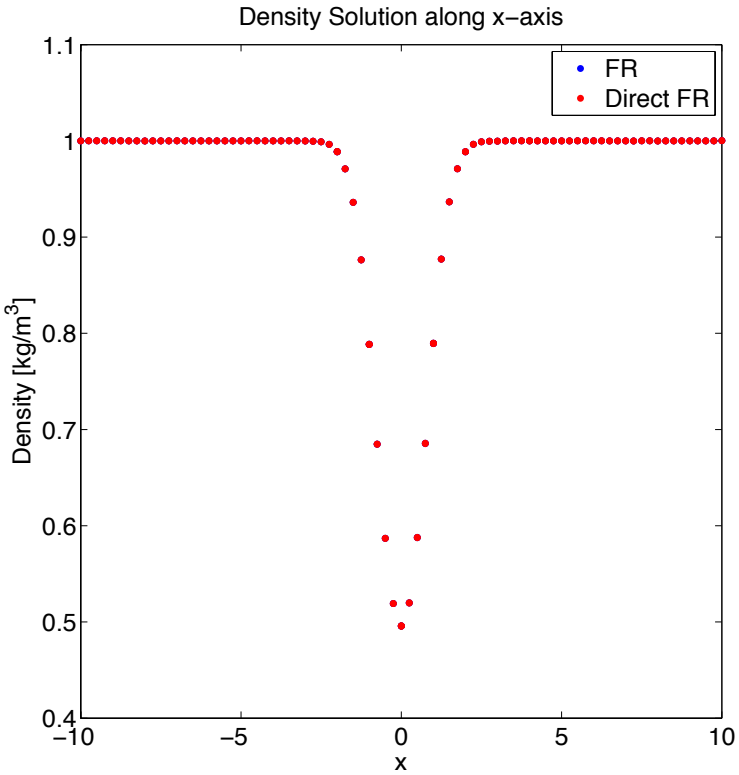

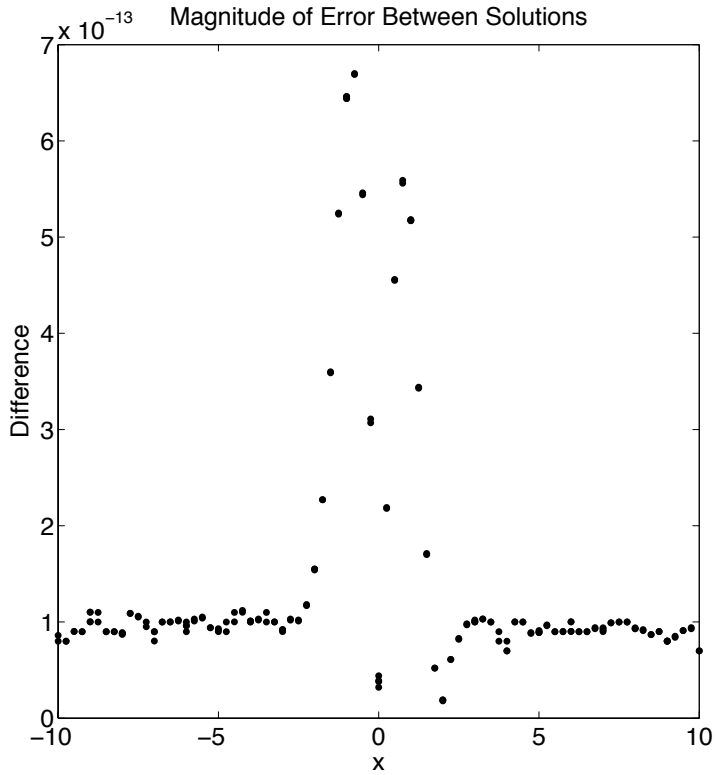

Scheme	Walltime [s]
FR	693.8270
Direct FR	592.9168
Percent Reduction	14.5%

Recovery of Additional Stable Schemes

- Beyond recovering the nodal DG scheme, numerical experiments indicate that DFR is stable with solution points located at the zeros of the Jacobi polynomial $P_n^{(\alpha,\beta)}(x)$, which is orthogonal on $[-1, 1]$ with respect to the weight:

$$W(x) = (1 - x)^\alpha (1 + x)^\beta$$

  for $0 < \alpha \leq 0.12$ and $\alpha = \beta$
- This may lead to a new family of schemes of interest.

Outline

Spectral resolution

The fraction of resolved wavenumbers for which constituent waves would be propagated with negligible numerical dispersion and dissipation

- The range of numerically resolved wavenumbers is limited by the grid resolution:

$$u^{\delta}(x,t)|_{\Omega^{\delta}} = \int_{k=-k_{max}}^{k_{max}} \hat{u^{\delta}}(k,\omega^{\delta}) e^{i(kx-\omega^{\delta}t)} \mathrm{d}k$$

- For wave propogation problems, the numerical approximation of derivatives provides the numerical dispersion relation

$$\omega^{\delta} = \omega^{\delta}(k)$$

Importance of spectral resolution in fluid phenomena

- High Reynolds number flows
  - In DNS, to accurately capture viscous dissipation at smallest scales, the numerical scheme must add minimal artificial dissipation at high wavenumbers (Moin 1997)
- Aeroacoustics
  - The calculation of far field noise requires acoustic waves to propogate undissipated and undispersed across several acoustic wavelengths (Tam 2001)
- Instabilites
  - Numerical dissipation at low wavenumbers can damp out physical instabilities, while negative numerical group velocities can lead to spurious bypass transition (Sengupta 2008)

FR formulation for 1-D convection

Consider the linear flux $f(u) = u$ on a uniform grid of unit spacing:

$$\frac{\partial u}{\partial t} + \frac{\partial u}{\partial x} = 0$$

Admit the fully upwinded interface flux so that the numerical update becomes:

$$\frac{d}{dt}\mathbf{u}_j^\delta = -2[\mathbf{C_0}\mathbf{u}_j^\delta + \mathbf{C}_{-1}\mathbf{u}_{j-1}^\delta]$$

for the j^{th} element, where $\mathbf{C_0}$ and $\mathbf{C_1}$ are discrete operators.

Bloch waves

The governing eqn. admits analytical solutions of the form:

$$u(x,t) = e^{ik(x-t)} = e^{ik(j-t)} e^{ik\frac{(r+1)}{2}}$$

where $r|_{\Omega_j} = 2\frac{x-x_j}{x_{j+1}-x_j} - 1$ represents the parent domain.

Project the exponential onto a polynomial basis:

$$\mathbf{u}_j^{\delta}(t) = e^{ik(j-a^{\delta}(k)t)}\mathbf{v}$$

Admitting the above numerical solution into the numerical update:

$$\frac{-2i}{k}\left(\mathbf{C_0} + e^{-ik}\mathbf{C_{-1}}\right)\mathbf{v} = a^{\delta}\mathbf{v}$$

Semi-discrete dispersion relation

The eigenvalue problem above results into $P+1$ eigenmodes.

- The eigenvalues relate directly to the numerical wavespeeds which provides for the *numerical semi-discrete dispersion relation*:

$$a_p^\delta(k) = a_{p_r}^\delta(k) + i a_{p_i}^\delta(k)$$

- The exact/analytical dispersion relation requires $a_r = 1$, $a_i = 0$
- The numerical solution can be expressed as:

$$\mathbf{u}^\delta(x,t) = e^{k a_{p_i}^\delta t} e^{ik(j - a_{p_r}^\delta t)} \mathbf{v}$$

providing the error terms:

Dispersion: $e^{ik(1-a_{p_r}^\delta t)}$

Dissipation: $e^{k a_{p_i}^\delta t}$

Eigenmodes for DG via FR on Gauss pts. for $P = 2$

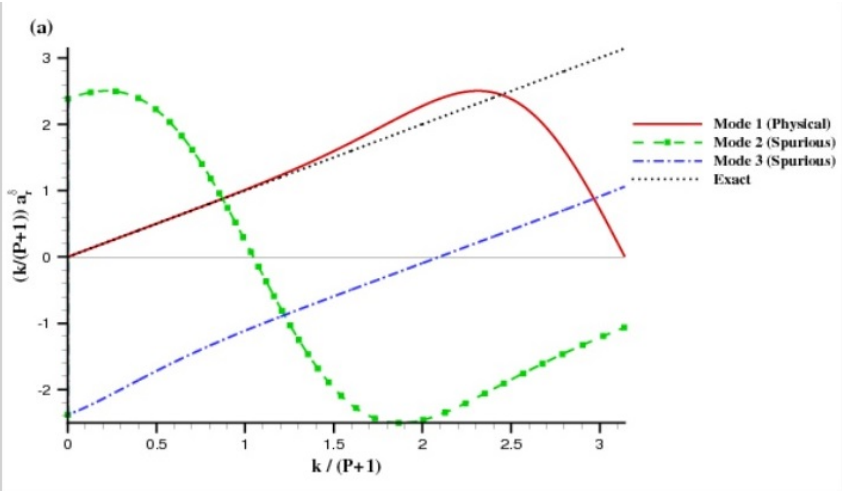

Real part of the numerical wavespeed

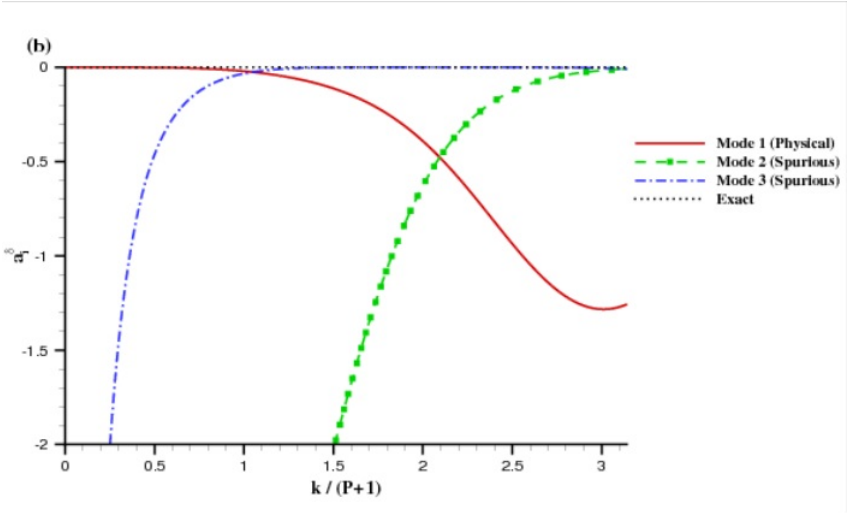

Imaginary part of the numerical wavespeed

Relative modal energies

The numerical initial condition is a projection of the exact one onto the polynomial basis. Due to the Lagrangian nature of the basis, it is exact at solution points:

$$\mathbf{v}_0 = e^{ik\frac{(r+1)}{2}} = \sum_{p=1}^{P+1} \mathbf{v}_p^{\delta} \lambda_p = \mathbf{V}\Lambda$$

- Complex weights λ_p relate to the contribution of each mode to the initial condition.

- A measure of *relative energy among modes* can be expressed as:

$$\beta_p = \frac{|\lambda_p|^2}{\sum_{q=1}^{P+1} |\lambda_q|^2}$$

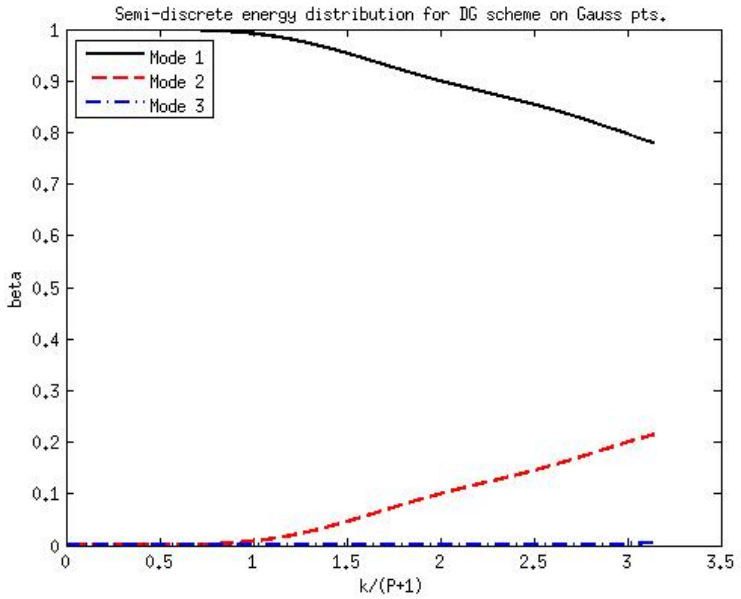

Choice of solution points

Numerical wavespeeds are independent of the choice of solution points. However, relative energies depend directly on the eigenvectors which are defined by the location of solution points

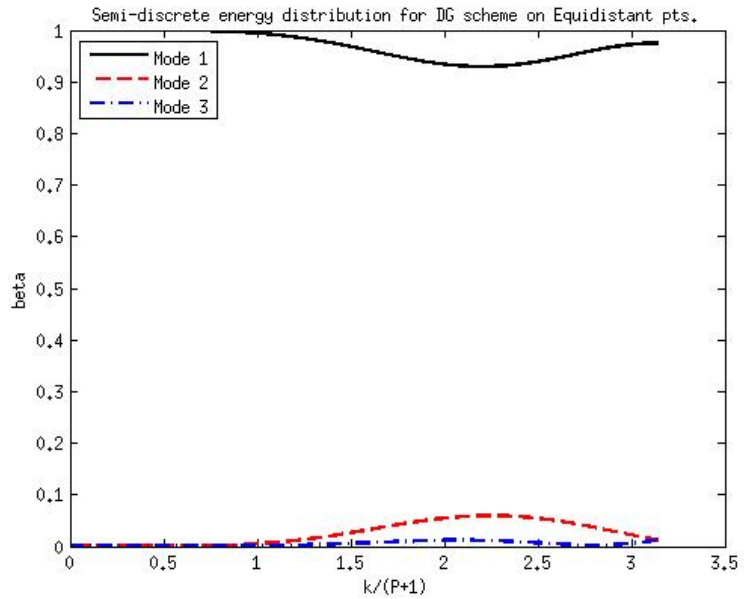

Relative modal energies for DG, P=2 on equidistant pts.

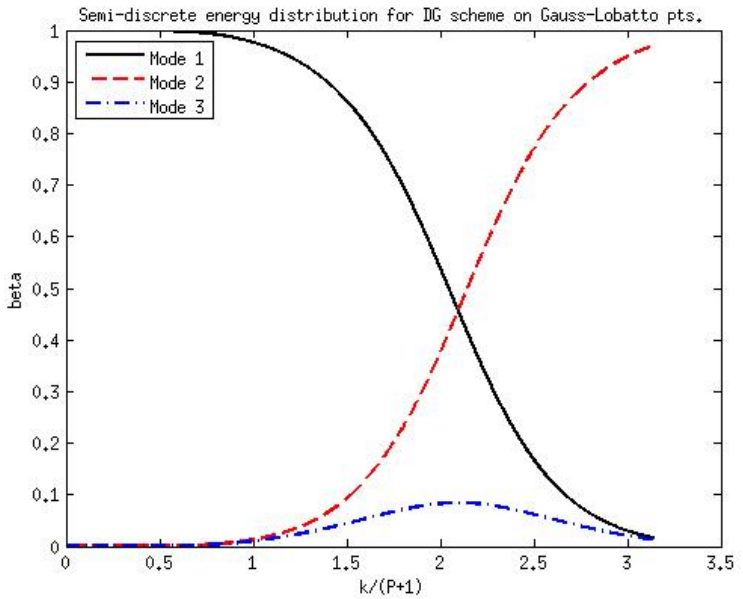

Relative modal energies for DG, P=2 on Gauss-Lobatto pts.

Wave propagation error

Spectral analyses of finite difference schemes have lead to the development of several *spectrally optimal compact schemes* that trade formal order of accuracy for better dispersion properties.

Tam (1993), Lele (1992), Ta'asan (1994), Kim (1996), Gaitonde (1997), Chu (1998), Adams (1996), Zhong (1998), Sengupta (2003)

- FR schemes
  - essentially upwinded - both real and imaginary parts
  - need to specify relative weights for dissipation and dispersion
  - convenient to select the actual wave propagation error:

$$
\begin{aligned}
|e_p(k,t)| &= |u^{ex}(k,t) - u^{\delta}(k,t)| \\
&= |e^{ik(x-t)} - e^{ik(x-c^{\delta}t)}| = |1 - e^{ik(1-c^{\delta})t}|
\end{aligned}
$$

Constrained minimization problem

An objective function for the optimization process can be specified as the energy weighted error in wave propagation measured at a characteristic time $t_c = 100h/c$:

$$\eta = \frac{1}{(P+1)^2} \sum_{p=1}^{P+1} \int_{k=0}^{(P+1)\pi} |1 - e^{i100k(1-a_p^{\delta}(k))}| \beta_p(k) \mathrm{d}k$$

where $\beta_p(k)$ is the relative modal energy of the p^{th} mode.

The optimzation problem can then be stated as follows:

$$\begin{aligned} \text{Min} \quad & \eta(g(r), P, \{r_0\}) \\ \text{subject to} \quad & a^{\delta}_{p_{imag}}(k) \leq 0 \quad \forall k \in [0, (P+1)\pi], \quad p = 1, 2, \ldots P+1 \end{aligned}$$

O-ESFR schemes

- Energy Stable Flux Reconstruction (ESFR) schemes (Vincent-Castonguay-Jameson 2011)
  - Proved to be stable for linear fluxes
  - Correction functions belong to a one-parameter 'c' family associated with the energy norm
  - Recovers DG for $c = 0$, SD for $c = \frac{2P}{(2P+1)(P+1)(a_P P!)^2}$
- ⋆ Optimal ESFR schemes (O-ESFR)
  - Can be obtained by optimizing over c for given P.

$$c_{DG} = 0$$

$$c_{SD} = 1.00 \times 10^{-3}$$

$$c_{OESFR} = 1.44 \times 10^{-4}$$

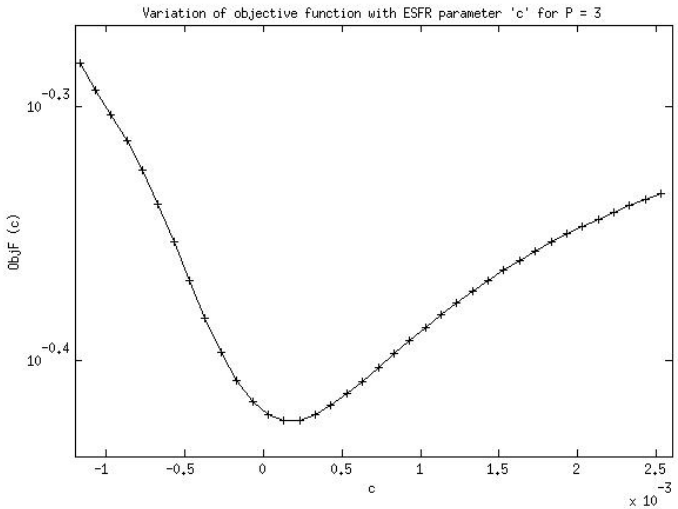

O-FR schemes

- General FR scheme
  - Generalized correction function on the left boundary

$$g_L(r) = \prod_{q=1}^{P} \frac{(r-\zeta_q)}{1+\zeta_q} \frac{(r-1)}{2}$$

  - The solution space of zeros $\{\zeta\}$ of g_L is of dimension P
  - Linear stability is not satisfied except in special subsets that may not form subspaces

⋆ Optimal FR schemes (O-FR) can be obtained by optimizing over the set of P available zeros subject to the constraint that the resulting scheme is stable.
$\rightarrow$ For $P = 1$, the O-FR scheme recovers the O-ESFR scheme
$\rightarrow$ For $P > 1$, the optimization procedure converges at zeros not traced by ESFR family.

Spectrally optimal FR schemes on Gauss pts. for $P = 5$

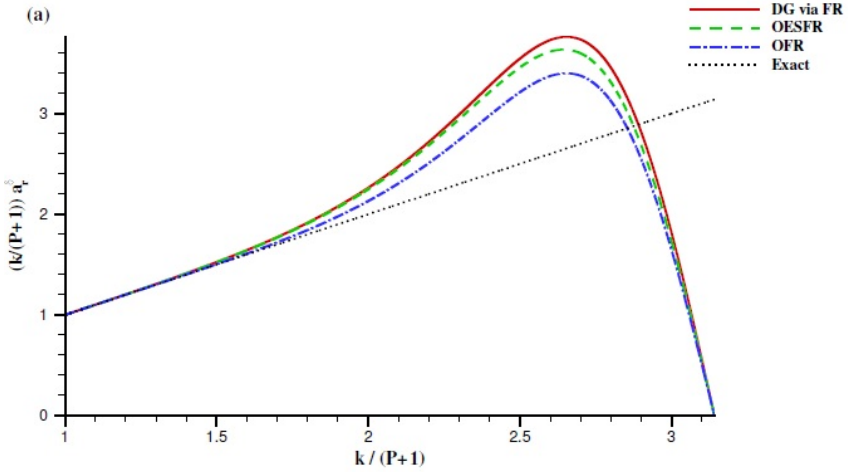

Real part of the numerical wavespeed

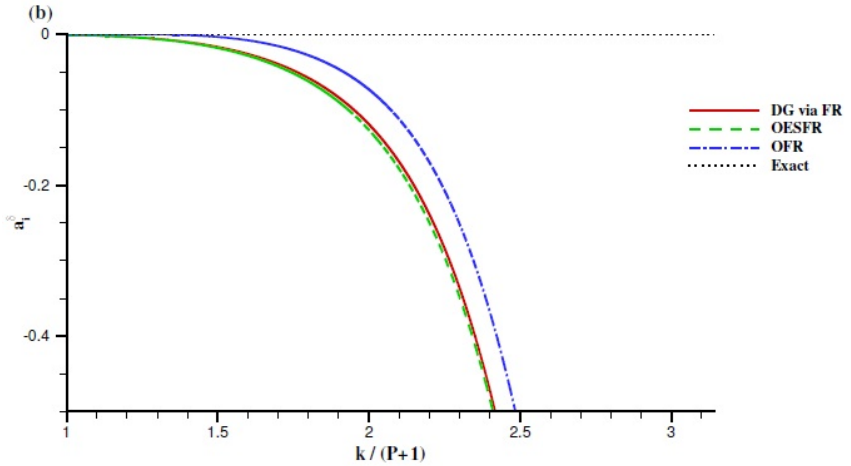

Imaginary part of the numerical wavespeed

Optimal correction functions for left boundary

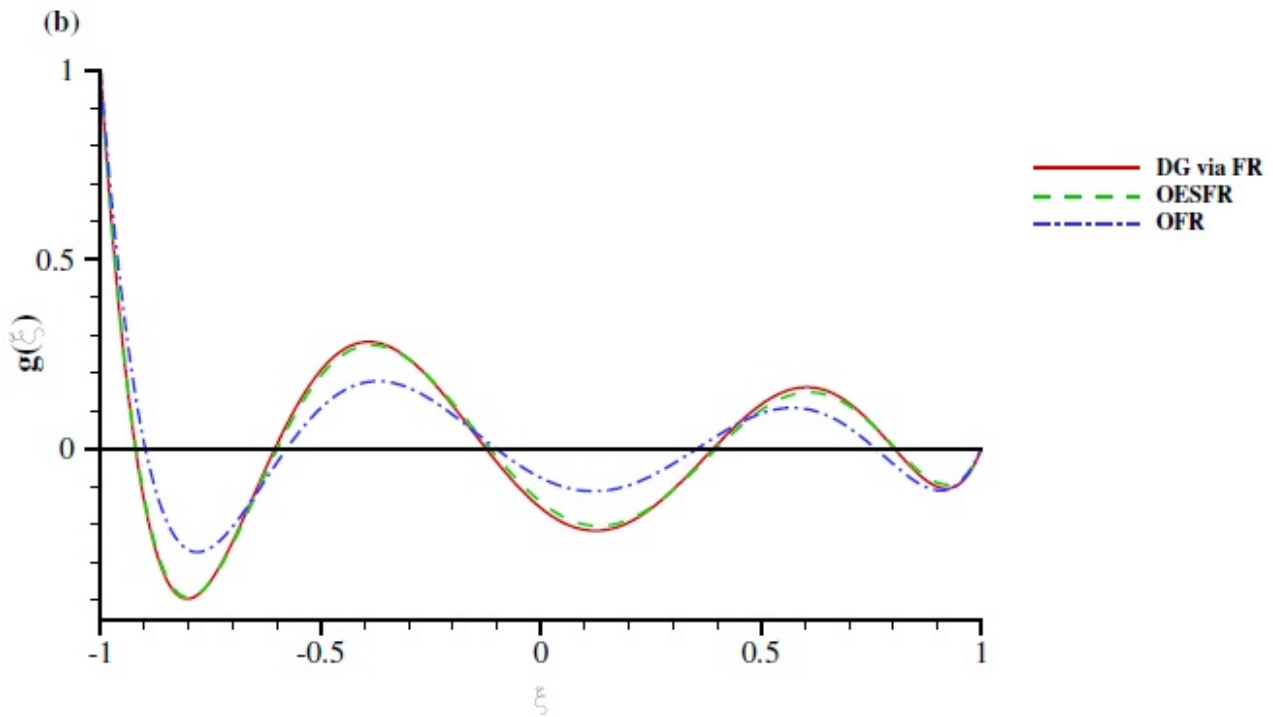

Left boundary correction functions for $P = 5$

Numerical integration: CFL restrictions

P	RK44				RK45			
	DG	OESFR	OFR	$c+$	DG	OESFR	OFR	$c+$
2	0.235	0.238	0.241	0.688	0.352	0.356	0.361	0.864
3	0.139	0.148	0.126	0.376	0.220	0.224	0.191	0.473
4	0.100	0.103	0.108	0.245	0.152	0.158	0.164	0.311
5	0.068	0.076	0.085	0.174	0.110	0.117	0.128	0.223

Limiting CFL values

- c_+ is the member of the ESFR family with highest stability limit (Vincent (2011))
- RK45 is the 4^{th} order accurate 5-stage RK scheme with enhanced stability region

1-D advection of a sharp Gaussian

6^{th} order standard and optimal FR schemes with an initial condition sharper than a single element

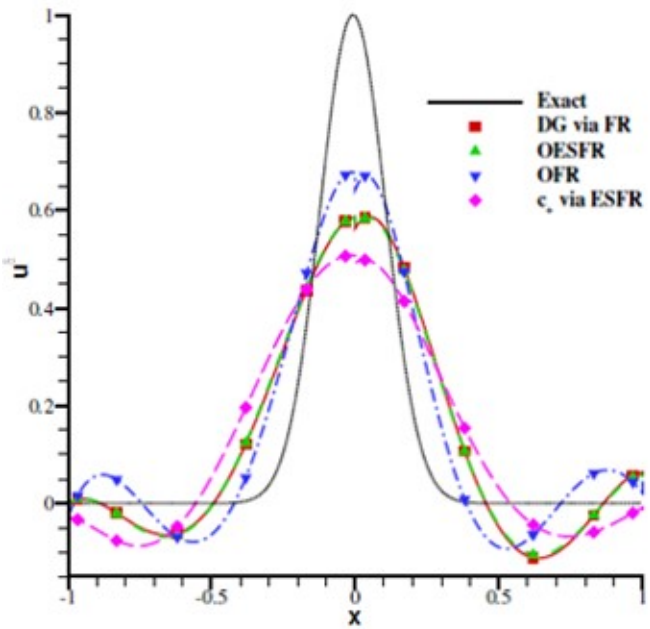

Exact and numerical solutions (across two elements) at the end of one period

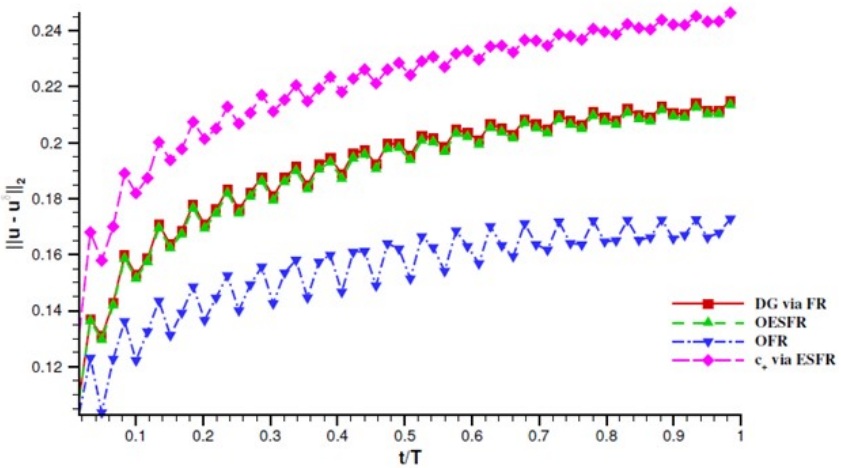

Evolution of numerical error across one period

1-D advection of a sharp Gaussian

6^{th} order standard and optimal FR schemes with finer meshes to accurately advect initial condition

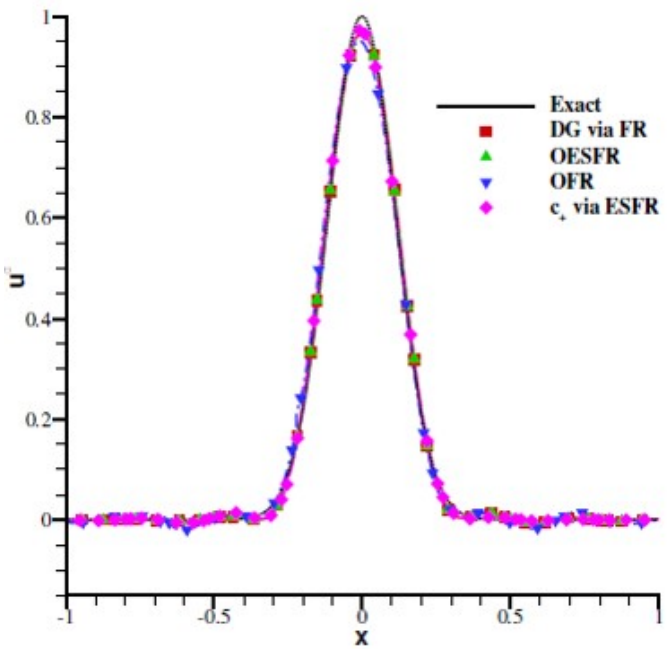

Exact and numerical solutions (across two elements) at the end of one period

Scheme	No. of elements
DG	61
Tridiag. implicit compact FD	57
c_+	76
OFR	45

No. of elements required for $< 5\%$ error in peak amplitude across one period

1-D advection of a high-wavenumber packet

6^{th} order standard and optimal FR schemes with an initial condition as a packet centered at half of Nyquist limit

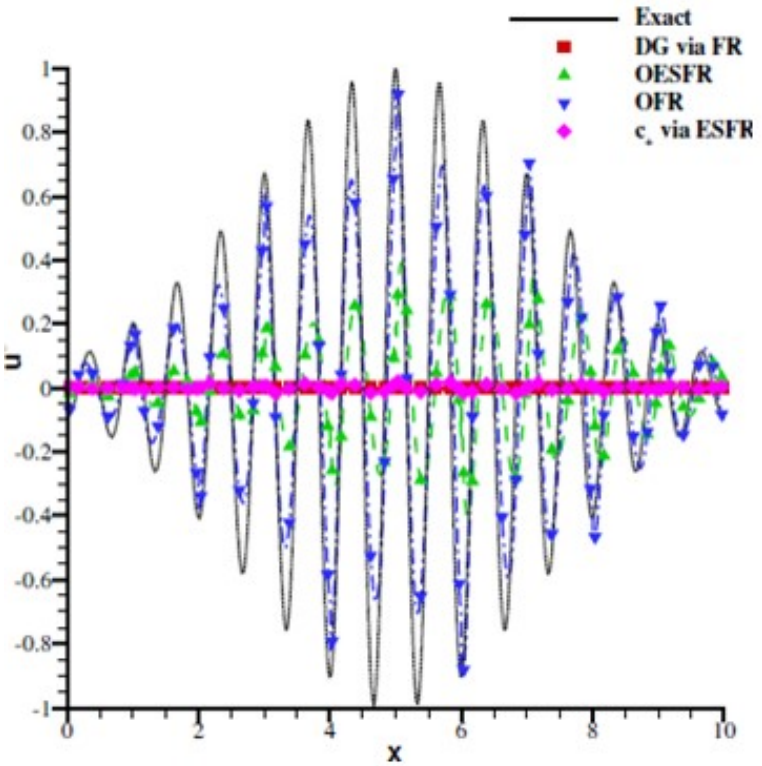

Exact and numerical solutions (across two elements) at the end of one period

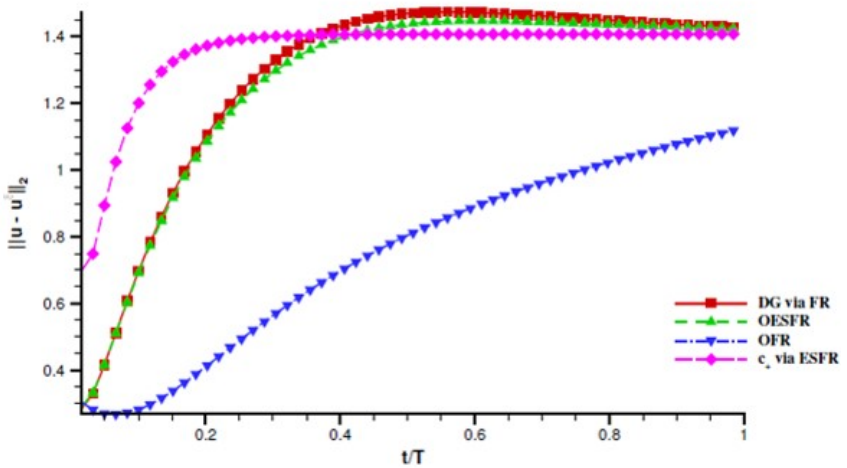

Evolution of numerical error across one period

Outline

HiFiLES: Open Source High Fidelity Large Eddy Simulation Code

- High-Order via Flux Reconstruction scheme
- RANS/LES
- GPU/CPU scalability
- Shock capturing
- Unstructured grids
- 4th order explicit time-stepping

Taylor Green Vortex - 64x64x64 mesh, 3rd order DG

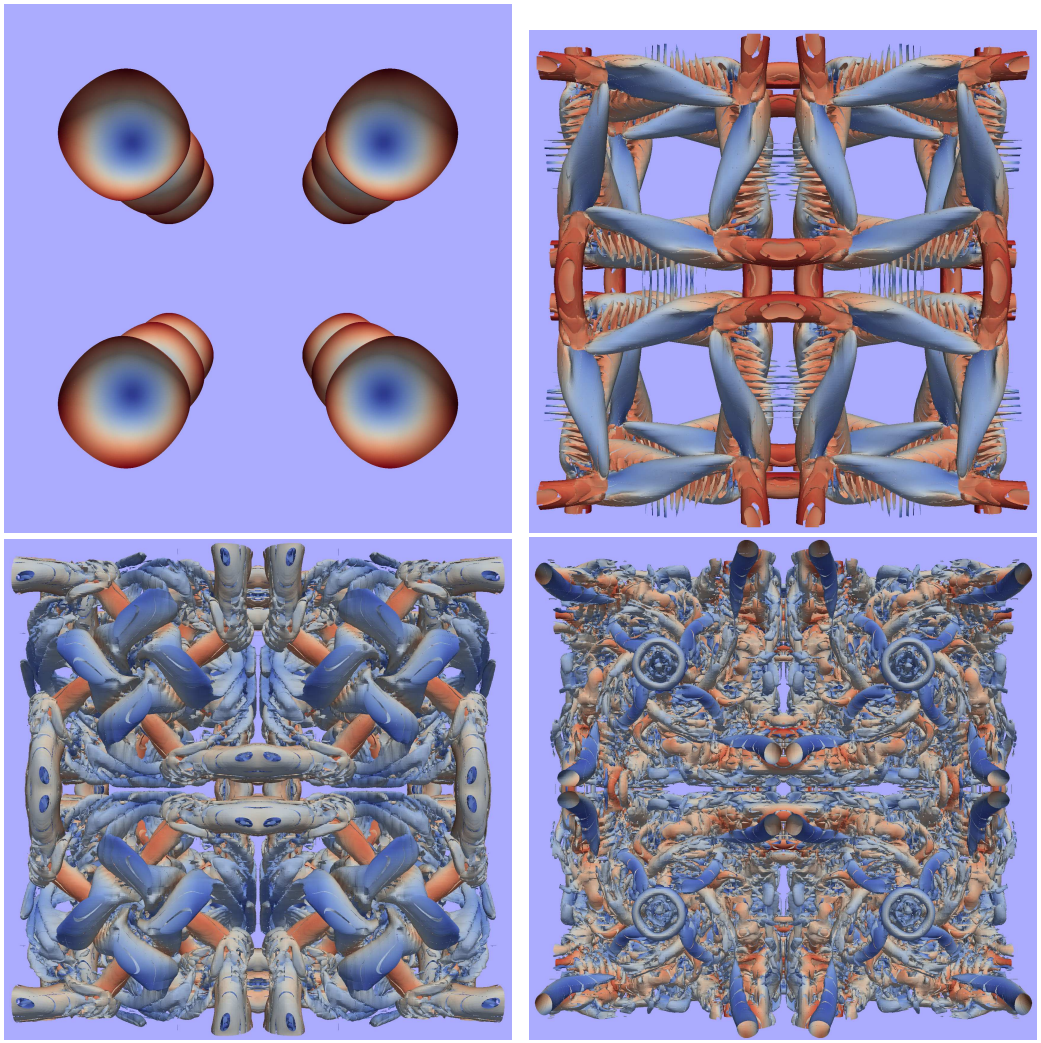

Q criterion colored by velocity magnitude at 2.5, 5.0, 7.5 and 10.75 seconds

Taylor Green Vortex - Comparison to Beck and Gassner DG

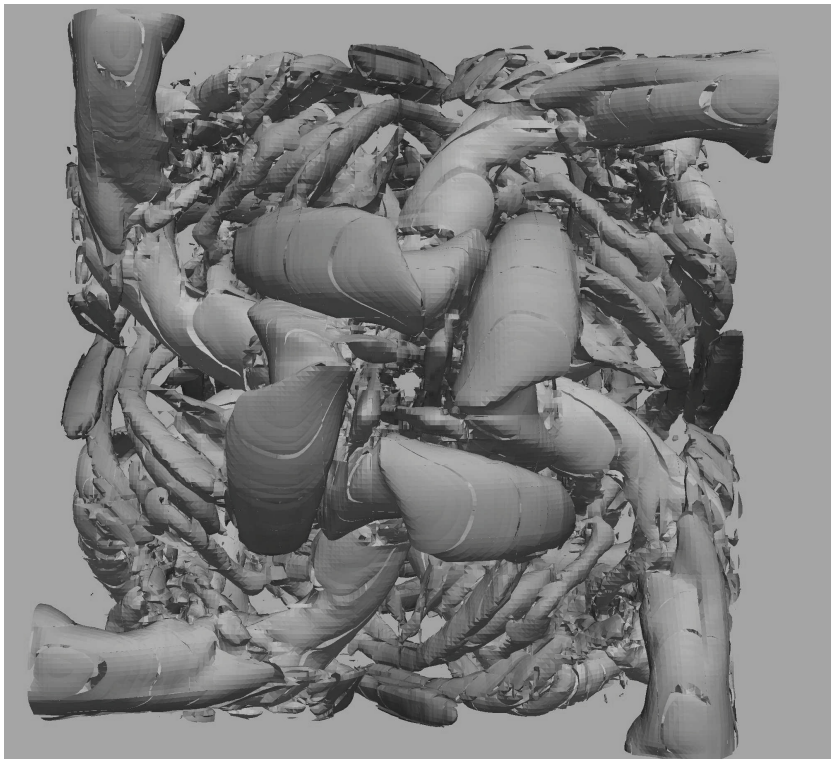

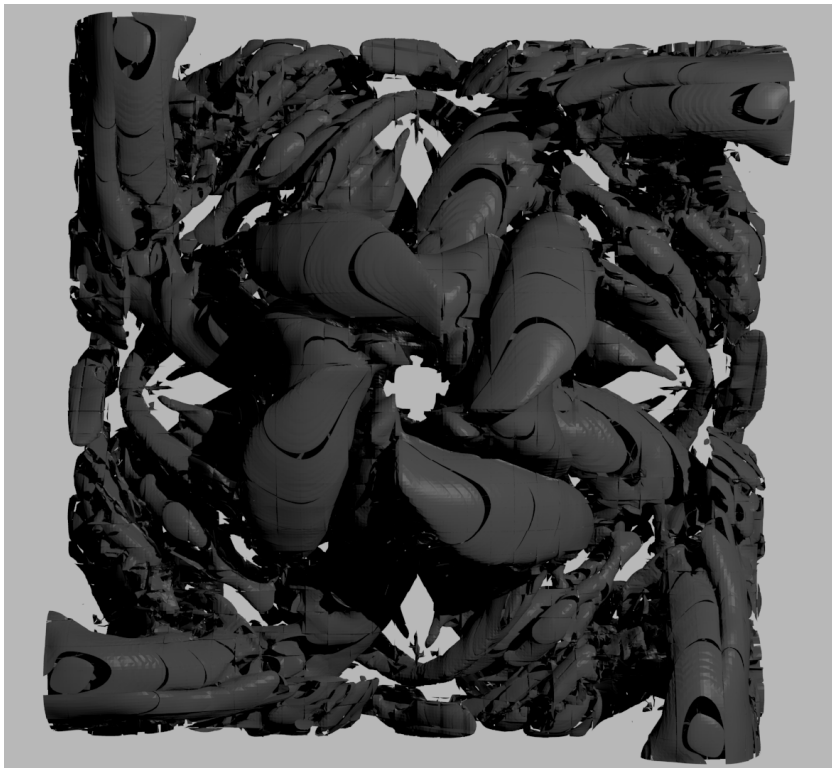

Left: 3rd order DG via FR (Bull and Jameson 2014)
Right: 3rd order filtered DG (Beck and Gassner 2012)

Taylor Green Vortex - Kinetic energy and dissipation rate

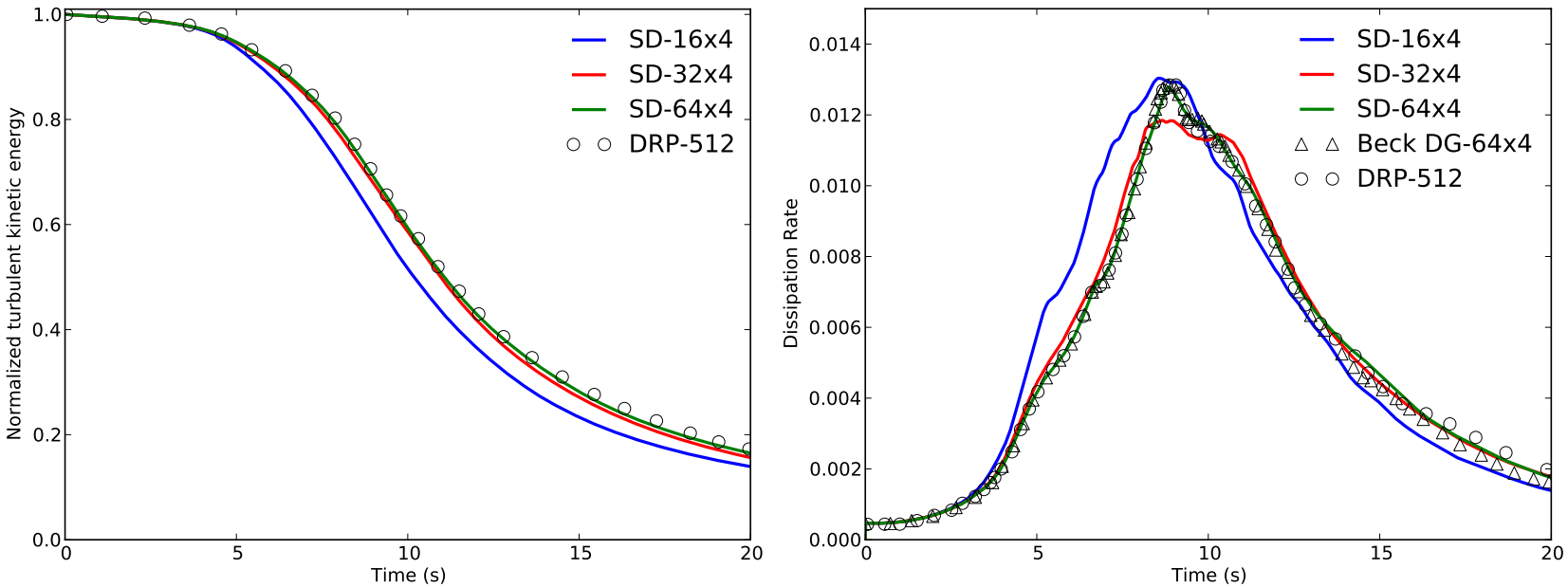

Kinetic energy k (left) and dissipation rate $-dk/dt$ (right) using 3rd order SD via FR on 16x16x16, 32x32x32 and 64x64x64 meshes vs. DG (Beck and Gassner 2012) and DNS using dispersion relation preserving (DRP) scheme (Debonis 2013)

Taylor Green Vortex - Vorticity-based dissipation rate

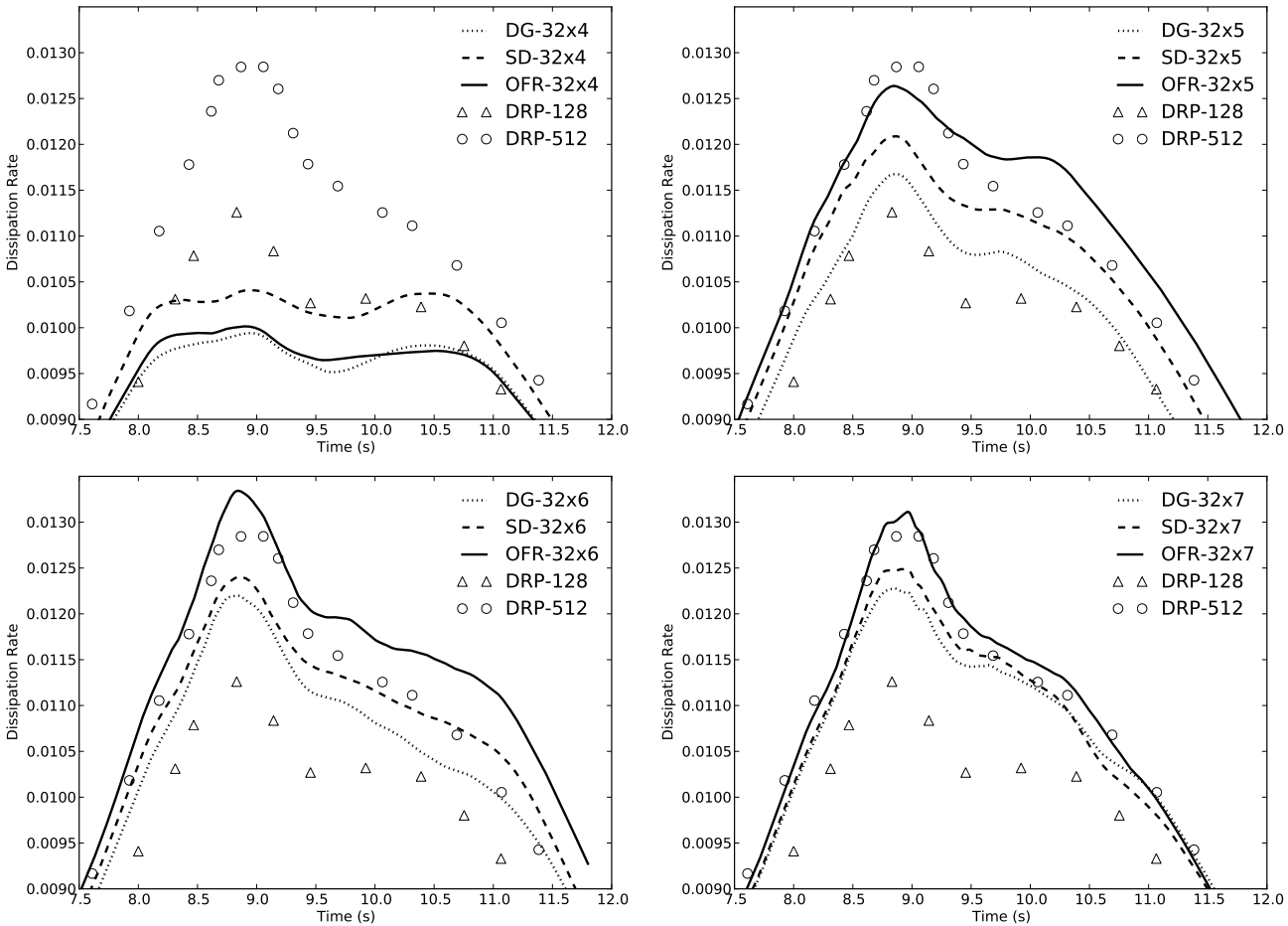

Vorticity-based dissipation rate using DG, SD and OFR schemes on 32x32x32 mesh at 3rd-6th orders (Bull and Jameson 2014)

Taylor Green Vortex - Energy spectra

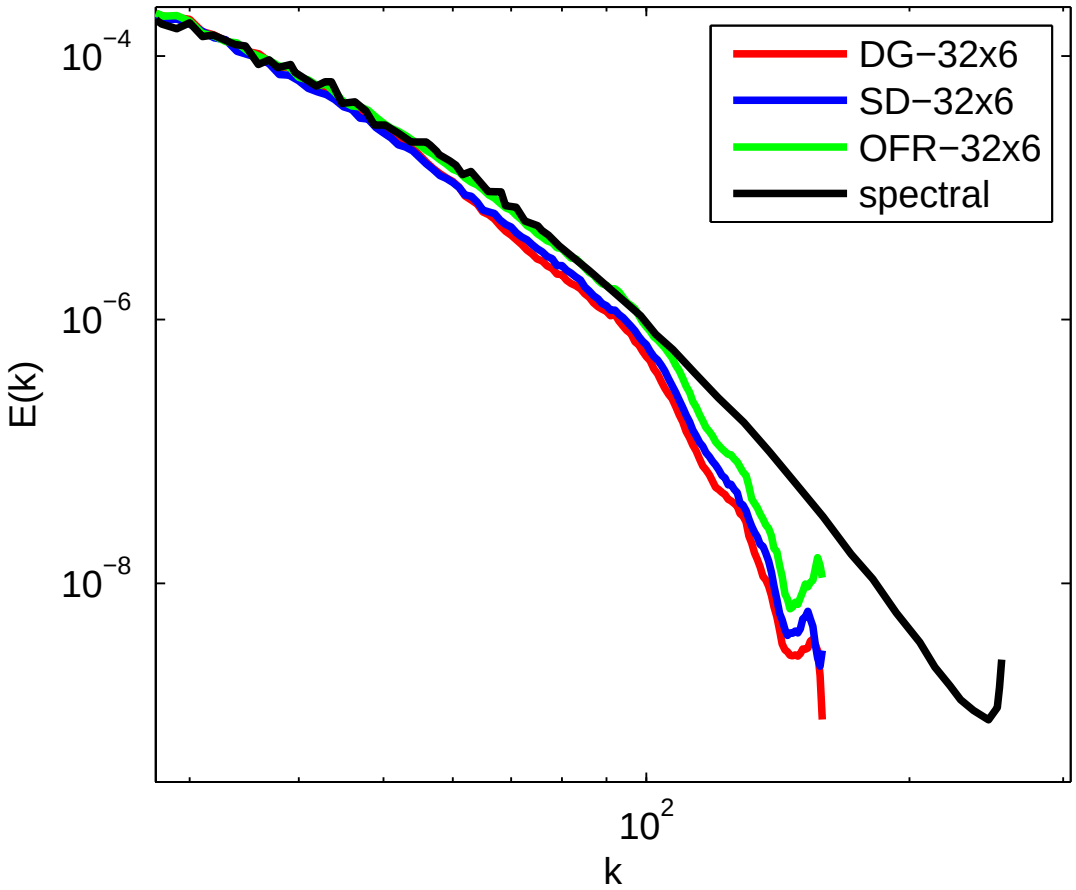

Close-up of energy spectrum at 9 seconds computed using 5th order DG, SD and OFR on 32x32x32 mesh vs. spectral DNS (Carton de Wiart et al. 2014)

Flow Over a Supersonic NACA 0012 Airfoil

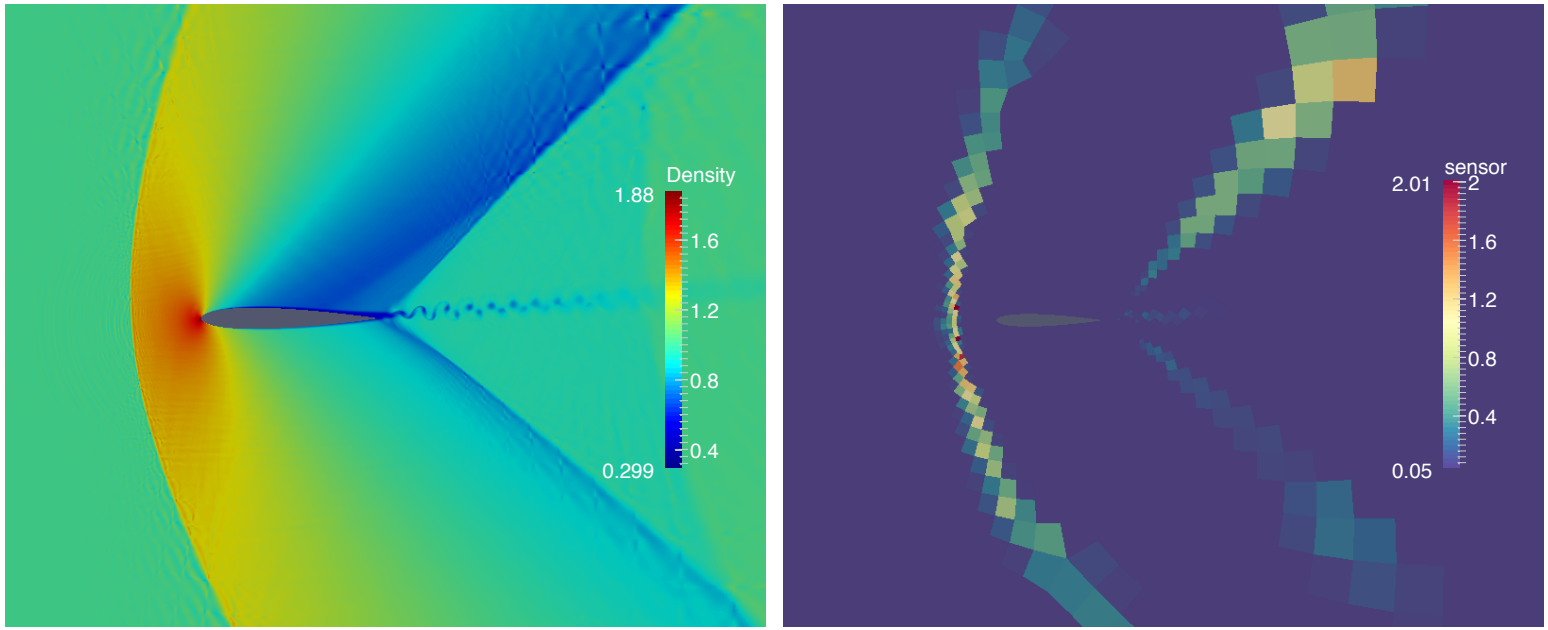

Density (left) and shock sensor (right) in flow over a NACA 0012 airfoil at Mach 1.2 and 5° AoA using 6th order FR

LES of Flow Over a Square Cylinder at $Re = 22,000$

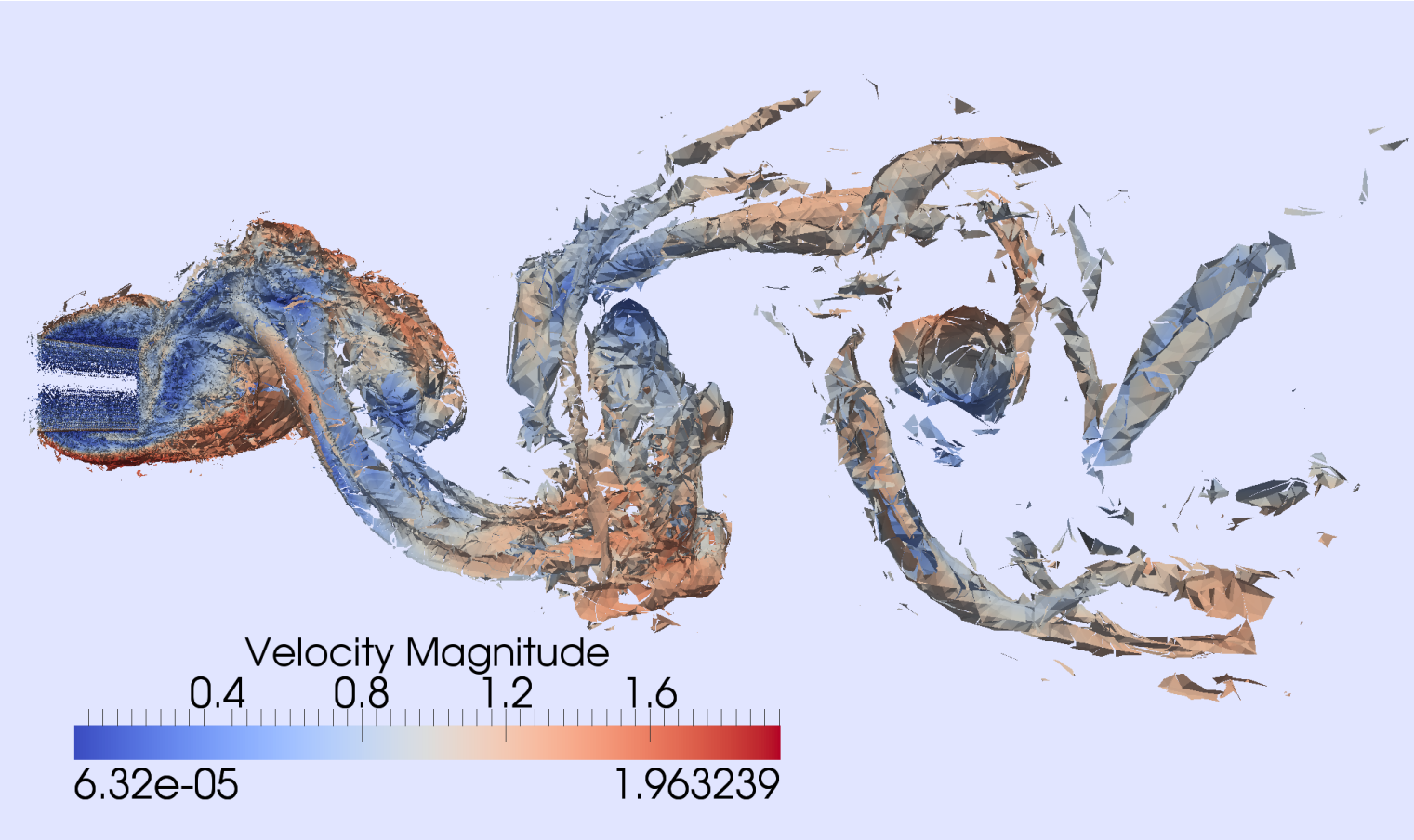

3rd order SD and WALE model on tetrahedral mesh with 130k elements. Isosurface of Q criterion colored by velocity magnitude.

Outline

Conclusions

- DFR is a simplification of nodal DG which may lead to a new family of schemes
- Spectrally optimal FR schemes allow higher accuracy without compromizing formal order, stability, or speed. This may enable the extension of FR to industrial applications in aeroacoustics and turbulence.
- Initial simulations of the Taylor-Green vortex using OFR (Bull et. al. 2014) have been shown to capture the inertial range better than conventional FR schemes.

Questions?